Published in final edited form as:
NMR Biomed. 2008 November ; 21(9): 928–940. doi:10.1002/nbm.1307.

Assessing Optic Nerve Pathology with Diffusion MRI: from Mouse to Human

Junqian Xu[1], **Shu-Wei Sun**[2], **Robert T. Naismith**[1], **Abraham Z. Snyder**[1,2], **Anne H. Cross**[1], and **Sheng-Kwei Song**[2]

1*Department of Neurology Washington University in St. Louis, St. Louis, Missouri, USA*

2*Department of Radiology Washington University in St. Louis, St. Louis, Missouri, USA*

Abstract

Optic nerve is often affected in patients with glaucoma and multiple sclerosis (MS). Conventional MRI can detect nerve damage but it does not accurately assess the underlying pathologies. Mean diffusivity and diffusion anisotropy indices derived from diffusion tensor imaging (DTI) have been shown to be sensitive to a variety of central nervous system (CNS) white matter pathologies. Despite being sensitive, the lack of specificity limits the ability of these measures to differentiate the underlying pathology in CNS white matter tissues. Directional (axial and radial) diffusivities, measuring water diffusion parallel and perpendicular to the axonal tracts, have been shown to be specific to axonal and myelin damages in mouse models of optic nerve injury, including retinal ischemia and experimental autoimmune encephalomyelitis (EAE). The progression of Wallerian degeneration has also been detected using directional diffusivities after retinal ischemia. However, translating these findings to human optic nerve is technically challenging. The current status of human optic nerve diffusion MRI, including the imaging sequences and protocols, are summarized herein. Despite lacking a consensus of the optimal sequence or protocol among different groups, increased mean diffusivity and decreased diffusion anisotropy has been observed in injured optic nerve from chronic optic neuritis patients. Decreased $\lambda_{\parallel}$, correlating with visual function and recovery, was observed recently in acute optic neuritis patients in a pilot study, suggesting the specificity of $\lambda_{\parallel}$ to axonal injury. From different mouse models of optic nerve injuries to the emerging studies on optic neuritis patients, directional diffusivities demonstrate great potential to be specific biomarkers for axonal and myelin injury.

Introduction

Optic nerve is a simple and well-defined white matter tract emanating from retinal ganglion cells. It is often affected in patients with multiple sclerosis (MS), where optic neuritis is frequently the first clinical symptom in MS [1-3]. Inflammation, demyelination, and axonal injury or loss are key components of MS pathologies [4]. The heterogeneity of lesion histopathology among individuals with MS is thought to account for the differences in the disease course and prognosis [4]. Although MS has been traditionally considered primarily a disorder of myelin, axonal loss can be prominent in some individuals. There is an emerging consensus that this can be a major contributor to long-term disability in MS [5,6]. Thus, an accurate assessment of these components of MS pathology is likely to improve stratification of the current treatments and prognostication of MS patients.

Requests for reprints: Sheng-Kwei Song, Biomedical MR Laboratory, Department of Radiology, Campus Box 8227, Washington University School of Medicine, 4525 Scott Avenue, St. Louis, MO 63110. Phone: (314) 362-9988; Fax: (314) 362-0526; E-mail: ssong@wustl.edu..

Although conventional MRI has been used to detect optic nerve atrophy and optic nerve sheath dilation [7-10], it fails to accurately assess the underlying pathophysiology preceding the irreversible structural damage. Other advanced MRI modalities, such as magnetization transfer (MT) [11-15] and T_2 based myelin water imaging [16-19], have been used to quantify white matter degeneration. In particular, quantitative MT showed promise in improving specificity to myelin injury [20-22]. However, the consensus of the capability of magnetization transfer or myelin water T_2 contrasts to differentiate axonal loss and myelin degeneration has yet to be established.

Diffusion tensor imaging (DTI) is widely recognized imaging modality to study the connectivity and integrity of white matter in central nervous system (CNS) tissues [23-25]. To accurately assess axonal and myelin damage, directional diffusivities derived from DTI have been proposed to serve as biomarkers of axonal and myelin damage [26-30].

Diffusion Tensor Imaging

Diffusion MRI measures the root mean square displacement of random Brownian motion of water molecules [31]. In a homogeneously isotropic medium with no restrictions, water molecules move in any direction with equal probability. The diffusion tensor can be represented by an isotropic diffusion displacement-probability sphere in this case. The scalar diffusion coefficient is sufficient to quantify the water diffusion. In contrast, for an anisotropic medium, such as biological tissues with various hindrances restricting water diffusion, the root mean square displacement of water molecules varies spatially. The diffusion weighted (DW) MR signal is dependent on the relative orientation of the diffusion-sensitizing gradient and the microstructures of the sample [32]. A diffusion-sensitizing gradient applied in a certain direction is only sensitive to the apparent diffusion coefficient (ADC) in that direction. Hence, a diffusion tensor description becomes necessary in such a situation, commonly achieved by a non-diffusion weighted (b_0) and a minimum of six diffusion weighted measurements in non-collinear and non-coplanar directions. The diffusion tensor can be represented by an anisotropic diffusion displacement-probability ellipsoid, characterized by three eigenvalues (λ_1, λ_2, and λ_3) and three eigenvectors in a local frame of each image voxel after matrix diagonalization. The average of the three eigenvalues is referred to as the mean diffusivity, MD. The sum of the three eigenvalues is the trace of the diffusion tensor, $Tr = 3 \times MD$. The diffusion anisotropy index, quantifying the degree of a preferred directionality for water displacement, is a measure of how much the diffusion ellipsoid deviates from a sphere. It reflects the structural anisotropy of porous media or tissue, in which water diffuses. Various anisotropy indices, such as fractional anisotropy (FA) and relative anisotropy (RA), are inter-convertible and have been summarized [33].

The MD and diffusion anisotropy indices derived from DTI allow for quantitative evaluation of the magnitude and degree of anisotropy of the random translational motion of water molecules. These two measures have been shown to be sensitive to a variety of brain pathologies [34-41]. However, despite being sensitive, the lack of specificity to the underlying CNS pathologies limits the use of these measures when differentiating the pathologies is clinically important. For example, reduced anisotropy and elevated MD, as often observed at pathological regions in CNS white matter from MS patients, do not always discriminate axonal damage from myelin pathology [26].

Directional Diffusivities as Biomarkers of Axonal and Myelin Injury

Eigenvalues of the diffusion tensor are scalar indices that describe water diffusion in a local, *i.e.*, voxel specific frame of reference coinciding with the geometry of white matter tracts. In CNS white matter, λ_1, the largest eigenvalue, represents the water diffusivity parallel to the axonal fibers. It is referred to as $\lambda_{\parallel}$, the axial diffusivity. The water diffusivities perpendicular

to the axonal fibers, λ_2 and λ_3, are averaged and referred to as $\lambda_\perp = (\lambda_2 + \lambda_3) / 2$, the radial diffusivity [26,27].

In white matter injury involving only myelin degeneration, we hypothesized that $\lambda_\parallel$ will not be affected, since the axon itself is not injured. In contrast, $\lambda_\perp$ will increase (diffusion anisotropy will decrease) reflecting the increased freedom of water Brownian motion perpendicular to axons due to the loss of myelin integrity.

We also hypothesized that axonal injury without (or prior to) demyelination will result in a decrease in $\lambda_\parallel$ (with or without a decrease in diffusion anisotropy). It is likely that $\lambda_\perp$ also decreases in axonal-only injury; however, the magnitude of this decrease in $\lambda_\perp$ is expected to be more difficult to detect since $\lambda_\perp$ is only about one fifth of the magnitude of $\lambda_\parallel$ in mouse CNS white matter [26,27,29,30,42,43].

In the extreme scenario in which the axon is extensively damaged with wide spread destruction of cellular structure and clearance of tissue debris, there is likely little restriction and hindrance to water diffusion, resulting in decreased anisotropy and increased freedom of motion for water molecules in all directions. If this occurs, $\lambda_\parallel$ and $\lambda_\perp$ will both increase and diffusion will become more isotropic, such as observed in chronic cerebral ischemia [44,45].

The above hypothesized alterations of directional diffusivity in CNS white matter injury are illustrated in optic nerve injury resulting from retinal ischemia and experimental autoimmune encephalomyelitis (EAE). The presentation of mouse models is followed by a detailed description of attempts in translating the findings in animal models to human.

Mouse Optic Nerve Pathology

Experimental Set Up and Imaging Protocol

Mice were anesthetized with isoflurane/O_2 (5% for induction and 2% for maintenance *via* a custom-made nose cone). The core temperature of mice was maintained at 37 °C using regulated, flowing warm water in a pad. Maintained at appropriate anesthesia, mice were placed in a custom-made, magnetic-resonance-compatible head holder with ear and tooth bars to immobilize the head. A 1.5-cm outer diameter circular surface coil was placed on top of the head to serve as the receiver for MR signal. The combined apparatus were placed in a custom-made cradle permitting the mouse to be placed at the center of magnet inside a 9-cm inner diameter Helmholtz coil (the radio frequency transmit coil). The above described arrangement was positioned in a second cradle that fits into an Oxford Instruments 200/330 (4.7 T, 33 cm clear bore) magnet.

A conventional, multi-slice, spin-echo imaging sequence, modified by adding the Stejskal-Tanner diffusion sensitizing gradient pair [46], was employed for acquiring the required series of diffusion weighted images (DWI) with repetition time (TR) 3 sec, echo time (TE) 50 msec, time between application of gradient pulses (Δ) 25 msec, slice thickness 0.5 mm, field of view 1.5 × 1.5 cm^2, data matrix 128 × 128 (zero filled to 256 × 256). Diffusion sensitizing gradient directions were: $[G_x,G_y,G_z]$ = [1,1,0], [1,0,1], [0,1,1], [−1,1,0], [0,−1,1], and [1,0,−1]. Two diffusion sensitizing factors, *b*-values = 0 and 785 s/mm^2, were used for the acquisition of the DWI series [32]. Five coronal slices of mouse brain were collected between – 0.5 to 2 mm of bregma for optic nerve studies. Regions of interest (ROI) were placed conservatively at the center of the optic nerves.

Noise induced bias to FA or individual eigenvalue is usually not of a concern for mouse studies because images of high signal-to-noise ratio (SNR > 30) are typically achieved. In addition,

we did not observe an improved accuracy in our measurement by using more diffusion encoding directions because there are no crossing-fibers in optic nerves.

Retinal Ischemia

Optic nerve degeneration resulting from retinal ischemia exhibits a distinct pathological profile with axonal injury preceding demyelination without significant destruction of overall axonal cytoskeletons [26,47,48]. *In vivo* DTI of optic nerve was performed longitudinally on mice having undergone transient retinal ischemia (Fig. 1). The optic nerve injury resulting from the death of retinal ganglion cells caused an early and prolonged decrease in diffusion anisotropy (Fig. 2). The temporal evolution of MD after retinal ischemia is similar to ADC changes reported in stroke [45] with a sharp decrease in MD observed as early as 3 days after retinal ischemia, followed by a gradual increase toward the control level at day 7 (Fig. 2). Most intriguingly, distinct patterns of $\lambda_{\parallel}$(early and prolonged decrease) and $\lambda_{\perp}$ (delayed and sustained elevation) during the progression of optic nerve degeneration were observed (Fig. 2) reflecting the expected pathological profile of axonal injury preceding myelin injury [26,47,48]. Thus, the pseudo-normalization of MD in this case is distinctly different from those seen in chronic stroke. The early decrease in MD reflects the decreased $\lambda_{\parallel}$. The pseudo-normalization at 7 days is a result of combined axonal injury and demyelination, the combined effect of the decreased $\lambda_{\parallel}$ and increased $\lambda_{\perp}$ resulting in little net changes in MD. These findings are consistent with the expected and histologically documented evolution of injury to the optic nerve, *i.e.*, axonal degeneration followed later by demyelination [26,47,48].

In addition to *in vivo* experiment, *ex vivo* MRI measurements of fixed tissues can provide high resolution images without *in vivo* physiological limitations such as limited scanning time, cardiac pulsation, and respiratory motions. However, careful validation is needed to account for the physiological and structural differences between *in vivo* and *ex vivo* tissue states [49]. For example, formalin fixation has been known for causing cross-linkage of proteins in excised tissues, leading to reduced T2 relaxation time. Besides *ex vivo* experiments are usually performed at room temperature which results in reduced water diffusivity compared to that measured at body temperature. However, diffusion anisotropy, normalized axial and radial diffusivity remained unchanged after tissue fixation [50]. To address the applicability of such practice in retinal ischemia, both *in vivo* and *ex vivo* DTI measurements were applied on optic nerves from mice having undergone transient retinal ischemia with matched histology [47]. At 3 days after ischemia, a decrease in $\lambda_{\parallel}$ was observed both *in vivo* (33%) and *ex vivo* (38%) in the injured optic nerve reflecting axon damage. At 14 days both *in vivo* and *ex vivo* measurements of $\lambda_{\perp}$ exhibited a significant increase reaching 220 - 240% control level in the injured optic nerve reflecting myelin damage. As expected, MD and diffusion anisotropy were not capable of detecting and differentiating axonal and myelin injury in the optic nerve. However, the axonal injury in optic nerve detected *in vivo* by the decreased $\lambda_{\parallel}$ was not seen *ex vivo* at 14 days after reperfusion. This decreased sensitivity of *ex vivo* DTI to axonal pathology at later stage of the injury cautions the application of *ex vivo* DTI measurements on fixed tissues for investigating *in vivo* pathophysiology.

Wallerian and dying-back degeneration play a significant role in many CNS diseases. Tracking the progression of Wallerian and dying-back degeneration may provide a better understanding of the evolution of these diseases. The use of DTI as a tool to investigate the CNS Wallerian and dying-back degeneration has become increasingly common [51-54]. Typically, mean diffusivity and diffusion anisotropy changes in white matter have been suggested to reflect the remote damage resulting from the primary insults to the gray matter. However, the damage identification based on statistical observations at a single location in the white matter tract could not differentiate the anterograde or retrograde nature of the injury [51,53,54]. In a recent longitudinal study taking advantage of the well-defined Wallerian degeneration of retinal

ischemia, the progression of Wallerian degeneration was evaluated by DTI in two functionally and structurally connected segments of a single axonal tract, the optic nerve and optic tract. The pattern of spatial and temporal evolution of the Wallerian degeneration as a result of the death of retinal ganglion cells was quantified by directional diffusivities [55]. At two weeks post-ischemia, more severe damage was present in the ipsilateral optic nerve than that in the contralateral optic tract (Fig. 3). Specifically, injured (ipsilateral) optic nerve showed a 32 – 40% decrease in $\lambda_{\parallel}$ with only a 21 – 29% decrease in injured (contralateral) optic tract, suggestive of more severe damage to the axons closer to the primary injury (retinal ganglion cells) than to those distant to it at two weeks after retinal ischemia. Similarly, 200 – 290% and 58 – 65% increases in $\lambda_{\perp}$ were observed in the injured (ipsilateral) optic nerve and injured (contralateral) optic tract, respectively, also suggesting more severe myelin loss in the proximal optic nerve than that in the distant optic tract and delayed myelin damage (Fig. 3). All DTI findings were quantitatively validated with immunohistochemistry [55].

Experimental Autoimmune Encephalomyelitis (EAE)

EAE is a widely used animal model [56] recapitulating many features of human MS [57]. EAE can be induced by immunization of susceptible animals with myelin proteins including myelin basic protein (MBP) [58], proteolipid protein (PLP) [59,60], and myelin oligodendrocyte glycoprotein (MOG) [61]. Optic neuritis is one of the phenotypes in EAE mice [62,63]. The optic nerves of the MOG-induced EAE mice were examined using *in vivo* DTI followed by immunohistochemisty. Chronic injury to the optic nerve from these mice involving both axonal injury and demyelination [43,64] has been quantified using directional diffusivities *in vivo* (Fig. 4). Our lab reported a 19% decrease in $\lambda_{\parallel}$ and 156% increase in $\lambda_{\perp}$ three month after immunization [43]. As suggested by counting phosphorylated neurofilament (pNF) and myelin basic protein (MBP) positive axons within the optic nerve (Fig. 5), the $\lambda_{\parallel}$ and $\lambda_{\perp}$ appeared to be both sensitive and specific for axonal injury and demyelination, respectively. Recently, Wu *et al.* [64] studied a EAE murine model in acute stage using *in vivo* DWI with diffusion sensitizing gradients parallel and perpendicular to the axonal tracts. They found that progressive acute axonal damage resulted in 23% decrease in $\lambda_{\parallel}$ at 20 days after immunization. They did not find significant changes in $\lambda_{\perp}$ during this acute period, which is consistent with the findings in the retinal ischemia model [26,47,55].

In summary, directional diffusivities ($\lambda_{\parallel}$ and $\lambda_{\perp}$) have been demonstrated to be specific to axonal injury and myelin damage in mouse models of optic nerve injury. In the optic nerve degeneration resulting from retinal ischemia, directional diffusivity is capable of detecting both axonal injury and demyelination, accurately depicting the temporal progression of the injury. In addition, directional diffusivities have been shown to detect and differentiate the severity between the proximal and distal injury in Wallerian degeneration. Directional diffusivities also accurately reflect the underlying axonal and myelin injury in the optic nerve and tract from chronic EAE mice. Based upon the successful application of directional diffusivities in mouse models of white matter injury, axial and radial diffusivities are potential biomarkers of axonal and myelin damage to be tested in the human optic nerve disorders.

Human Optic Nerve

Challenges of Imaging Human Optic Nerve

The diameter of the mouse and human optic nerve is about 0.3 – 0.4 mm and 3 – 4 mm, respectively. Thus, high resolution is required to avoid partial volume effect when imaging the optic nerve. One of the most critical issues facing human optic nerve MRI is the tradeoff between high image resolution, to avoid partial volume effect, and adequate signal-to-noise ratio (SNR), necessary for reliable diffusion measurements. For mouse optic nerve imaging, a lengthy acquisition of the anesthetized animal with the use of a surface receiver coil helped to

achieve the necessary high resolution DTI measurements while maintaining sufficient SNR. However, the long DTI acquisition of the optic nerve in mice is not practical in human.

The human optic nerves are wrapped by several layers of membranes, *i.e.*, nerve sheath, and immediately surrounded by cerebrospinal fluid (CSF) [65]. In atrophic nerves, the nerve itself could detach from the nerve sheath with CSF filling the intermediate space. Thus, CSF suppression is desirable and even indispensable for imaging atrophic nerves. The intra-orbital portion of the optic nerve and the nerve sheath are also surrounded by the orbital fat, necessitating fat suppression. Partial volume effect from CSF, chemical shift effect from fat, and the susceptibility artifacts due to air/tissue interfaces at nearby sinuses all contribute to the technical difficulties of imaging human optic nerves. Motion artifacts resulting from eye ball and/or bulk head movements further complicate optic nerve imaging. These constraints have made the applications of diffusion MRI to the human optic nerve a challenging endeavor. Surmounting these obstacles requires the consideration of unconventional diffusion pulse sequence design. Since not all concerns can be addressed in a single sequence, necessary compromises have to be made to effectively address the clinical question.

Despite the technical challenge, MRI of optic nerve offers the advantage in that visual function is directly measurable. Hence, MRI results can be correlated with visual functions and optical coherence tomography (OCT) measured retinal nerve fiber layer thickness [66]. Clinical visual function tests, such as visual acuity, contrast sensitivity [67], visual evoked potential (VEP) [68,69] are direct measures of specific functions of the visual pathway specialized for transmitting visual representations to higher brain centers.

Imaging Sequences

Diffusion weighting with spin-echo (SE) [70], fast spin-echo (FSE) [71] and single shot spin-echo echo planar imaging (SE-EPI) [72-74] have been previously used to image the optic nerve. Due to its high SNR efficiency, SE-EPI is the sequence of choice among most research groups. In order to improve image resolution while reducing image distortion of EPI sequence in human optic nerve imaging, on the basis of SE-EPI, the inner volume imaging (IVI) or reduced field of view (rFOV) technique [75-79] has been recently presented. The original version of IVI technique used one 90° slice selective excitation pulse and one 180° slab selective refocusing pulse in orthogonal directions to select a rectangular volume of interest [80]. The disadvantage of the original IVI technique is its low imaging efficiency because the magnetization outside of the selected slab was inverted by the 180° pulse. This makes interleaved multi-slice data acquisition problematic. Zonal oblique multislice (ZOOM) EPI method, a modified IVI technique applying the selective pulses in oblique angles [81], was subsequently developed enabling the interleaved multi-slice acquisition with judicious selections of oblique angles. This technique has been employed with diffusion encoding [75]. However, ZOOM-EPI leaves slice gaps in the anatomy of interest because spatial saturation pulses were required to ensure a rectangular volume excitation. Interleaving slice groups can provide continuous coverage with compromise in imaging efficiency. A solution to this shortcoming is to apply a second slab selective 180° pulse at the end of the imaging module [82]. This second selective 180° pulse has the effect of restoring the magnetization inverted by the first 180° pulse back to the positive B_0 field axis before subsequent slice selective excitations. This technique was further coupled with twice refocusing spin echo (TRSE) [83] diffusion weighting scheme (Fig. 6) recently for diffusion measurements [79,84]. To further reduce image distortion associated with EPI, improved post-processing techniques, using segmented or stimulated echo planar imaging (STEPI) [85] module, or replacing EPI with imaging modules less sensitive to distortions from off-resonance effects may be necessary. Potentially useful imaging modules with minimum distortion include line scan [86-88], turbo fast low flip angle shot (turbo FLASH) [89], and its closely related turbo stimulated echo acquisition mode (turbo STEAM) [90-92]. However, SNR

inefficiency limits application of these techniques at the current magnetic field strength used for *in vivo* human imaging. Alternatively, the recently developed rapid acquisition by sequential excitation and refocusing (RASER) sequence [93] offers reasonable SNR compared to EPI, substantially reduced susceptibility effect, and no blurring from *k*-space filtering. It is also inherently suitable for limited FOV application. When this sequence is adapted with diffusion gradients, it may be a potential candidate for imaging optic nerve.

Imaging Protocols

Different approaches have been adopted to address the many challenges faced in human optic nerve diffusion MRI as mentioned before. The resulting various imaging protocols derived from different research groups warrant a detailed description as these may have implications on interpreting results. What is common among most of groups is the choice of a maximum *b* value of about 600 s/mm^2 [71,73,76-79]. Despite being suboptimal for diffusion sensitizing human brain white matter, the relatively low *b* value ensures sufficient SNR in diffusion weighted images. A minimum number of directions for diffusion tenor encoding is typically used due to imaging time constraints when multiple averages are necessary to improve SNR. Even after signal averaging, the relatively low SNR at the required resolution may lead to an overestimation of FA. ROIs are usually placed away from the unmyelinated optic nerve head and at the center of the optic nerve to avoid CSF contamination, which may lead to an underestimation of FA and an overestimation of MD.

Wheeler-Kingshott and colleagues employed CSF suppression and a 2D spectral spatial selective excitation pulse in ZOOM-EPI diffusion sequence. This modification showed promising results from healthy volunteers [78] and chronic optic neuritis patients [76,77] on 1.5 T scanners. DTI data were collected using head transmit-receive coils with a voxel size of 1.25 × 1.25 × 4 mm^3 in coronal plane. Despite being less sensitive than phased array or surface coils, the head coil offered a relatively high signal penetration for imaging the optic chiasm [94]. The signal loss due to inversion preparation for CSF suppression was mitigated by signal averaging and noise bias correction during post processing [75].

In a pilot study, our lab performed studies on healthy volunteers on a 3 T scanner using the recently implemented IVI with TRSE diffusion weighting [79]. MR data were acquired in transverse plane with a transmit head coil and a 4-element flexible phased array optic nerve receiver coil [94]. Isotropic voxels of 1.3 × 1.3 × 1.3 mm^3 were employed to minimize CSF contamination and only voxels in the center of nerve were used for quantification. CSF suppression was not used in this study due to the needed SNR at such a high image resolution. Distortions associated with the high-resolution EPI sequences were minimized by the reduced echo train length using the IVI technique (Fig. 7). Fat suppression was achieved by a chemical shift selective fat suppression pulse with dephasing gradients at the beginning of the pulse sequence and gradient reversal technique during the spin echo evolution (Fig. 6) [95,96].

Chabert *et al*. used the non-CPMG FSE sequence [97] to study a cohort of healthy volunteers at 1.5 T [71]. MR data were acquired in transverse plane with a 3 inch diameter surface coil over a single eye. A voxel size of 0.94 × 0.94 × 3 mm^3 was chosen without CSF suppression. The FSE nature of the sequence reduces artifacts related to off-resonance effects. However, due to the long echo train length, this sequence is more sensitive to motion and T_2 blurring. In addition, chemical-shift artifacts were significant in this sequence, probably due to the non-ideal refocusing pulse profile and the quadratic phase modulation of the refocusing pulses.

Healthy Control

Despite consistent measures of optic nerve diffusion parameters within the individual research group [75-78,98], minor discrepancies in the reported normative values exist among different

groups employing different imaging sequences and protocols (Table 1, only DTI studies with sufficient statistical power were summarized). The observed discrepancies may arise from the difference in SNR, imaging orientations (transverse vs. coronal), spatial resolution, and CSF/fat suppression. Currently, a consensus regarding the optimal optic nerve diffusion imaging protocol has yet to be reached.

In spite of the difficulty in comparing diffusion parameters among different groups, trends of changes or relative changes in diffusion parameters between the control and injured optic nerve exist.

Optic Neuritis

Trips *et al.* [77] studied a heterogeneous cohort of chronic optic neuritis patients with previous unilateral attack using the ZOOM-EPI diffusion sequence/protocol. There was not a significant difference between unaffected contralateral nerves and that from the healthy control. They observed a 93% increase in $\lambda_{\perp}$, a 49% increase in MD, and a 35% reduction in FA in the affected optic nerve compared with that from the healthy control ($p < 0.001$) or the contralateral nerve ($p < 0.001$). Only a marginal 13% increase in $\lambda_{\parallel}$ was observed in the affected nerve. The change in $\lambda_{\parallel}$ is not statistically significant ($p = 0.13$) compared with those in the healthy control, while it is significant ($p = 0.04$) compared with the contralateral nerves. The dramatic increase in $\lambda_{\perp}$ and marginal change in $\lambda_{\parallel}$ are similar to those observed in the chronic EAE mouse model. This study did not find an association between DTI indices and visual functions, possibly due to the patient heterogeneity. In contrast, sixteen chronic patients were examined one year after optic neuritis attack by the same group in a separate study [76]. The increased mean ADC in the affected nerve correlated with measures of the visual function (visual acuity, visual field, and color vision) and electrophysiological parameters (VEP amplitudes and latencies). Unfortunately, neither anisotropy nor directional diffusivity data was measured in this second study. Comparing the results from these two studies is difficult, because tissue injury due to demyelinating disease is a dynamic process. It is expected that diffusion parameters will change over time reflecting the underlying structural changes. The timing of diffusion imaging, as well as whether there was a pre-existing injury within the optic nerve should be taken into account for proper interpretation and comparison of diffusion MRI results. Although there has not been reported applications of directional diffusivities on acute optic neuritis patients, recent preliminary data shows acute decrease in $\lambda_{\parallel}$ correlating with long term recovery [99].

Conclusion

Directional diffusivities ($\lambda_{\parallel}$ and $\lambda_{\perp}$) have shown to be specific to axonal injury and myelin damage in mouse models of optic nerve injuries. Optic nerve degeneration resulting from retinal ischemia exhibits a distinct pathological profile with axonal injury preceding demyelination without significant destruction of overall axonal cytoskeletons. This presents a unique opportunity for longitudinal DTI studies, both *in vivo* and *ex vivo*, to access the different optic nerve pathologies using directional diffusivities. In addition, the progression of Wallerian degeneration from optic nerve to optic tract can also be detected by directional diffusivity after retinal ischemia. In the EAE mouse model, quantitative immunohistochemistry shows that the $\lambda_{\parallel}$ and $\lambda_{\perp}$ are both sensitive and specific to axonal injury and demyelination.

However, translating these results from mouse to human optic nerve faces various technical challenges, among them the trade-off between high image resolution and adequate SNR is the most crucial. Successful human optic nerve imaging requires unconventional diffusion sequence design. Wheeler-Kingshott group has shown diffusion weighted images and DTI measurements using diffusion sequences implemented with inner volume imaging techniques. Despite the lack of a consensus on diffusion sequences or protocols for human optic nerve

imaging among different groups, increased mean diffusivity and decreased diffusion anisotropy have been observed in injured optic nerve from chronic optic neuritis patients.

Directional diffusivities have been demonstrated to be a biomarker of axon and myelin injury in mouse models of optic nerve injury. If the observation in mice can be realized in the emerging studies of optic neuritis patients, directional diffusivities will improve the stratification of current treatments and prognostication of not only optic neuritis patients but also MS patients in general and patients with other CNS white matter disorders.

Acknowledgment

This study was supported partly by grants provided by NMSS RG-3670, RG-3864 and CA-1012, and NIH R01-NS-054194.

References

1. Chan JW. Optic neuritis in multiple sclerosis. Ocul Immunol Inflamm 2002;10(3):161–186. [PubMed: 12789593]
2. Rocca MA, Hickman SJ, Bo L, et al. Imaging the optic nerve in multiple sclerosis. Mult Scler 2005;11 (5):537–541. [PubMed: 16193891]
3. Atkins EJ, Biousse V, Newman NJ. The natural history of optic neuritis. Rev Neurol Dis 2006;3(2): 45–56. [PubMed: 16819420]
4. Lucchinetti C, Bruck W, Parisi J, Scheithauer B, Rodriguez M, Lassmann H. Heterogeneity of multiple sclerosis lesions: implications for the pathogenesis of demyelination. Ann Neurol 2000;47(6):707–717. [PubMed: 10852536]
5. Trapp BD, Bo L, Mork S, Chang A. Pathogenesis of tissue injury in MS lesions. J Neuroimmunol 1999;98(1):49–56. [PubMed: 10426362]
6. Bjartmar C, Trapp BD. Axonal degeneration and progressive neurologic disability in multiple sclerosis. Neurotox Res 2003;5(12):157–164. [PubMed: 12832230]
7. Hickman SJ, Brex PA, Brierley CM, et al. Detection of optic nerve atrophy following a single episode of unilateral optic neuritis by MRI using a fat-saturated short-echo fast FLAIR sequence. Neuroradiology 2001;43(2):123–128. [PubMed: 11326556]
8. Hickman SJ, Brierley CM, Brex PA, et al. Continuing optic nerve atrophy following optic neuritis: a serial MRI study. Mult Scler 2002;8(4):339–342. [PubMed: 12166505]
9. Hickman SJ, Toosy AT, Jones SJ, et al. A serial MRI study following optic nerve mean area in acute optic neuritis. Brain 2004;127(Pt 11):2498–2505. [PubMed: 15342363]
10. Hickman SJ, Miszkiel KA, Plant GT, Miller DH. The optic nerve sheath on MRI in acute optic neuritis. Neuroradiology 2005;47(1):51–55. [PubMed: 15633052]
11. Thorpe JW, Barker GJ, Jones SJ, et al. Magnetisation transfer ratios and transverse magnetisation decay curves in optic neuritis: correlation with clinical findings and electrophysiology. J Neurol Neurosurg Psychiatry 1995;59(5):487–492. [PubMed: 8530932]
12. Filippi M, Rocca MA. Magnetization transfer magnetic resonance imaging of the brain, spinal cord, and optic nerve. Neurotherapeutics 2007;4(3):401–413. [PubMed: 17599705]
13. Inglese M, Rovaris M, Bianchi S, et al. Magnetic resonance imaging, magnetisation transfer imaging, and diffusion weighted imaging correlates of optic nerve, brain, and cervical cord damage in Leber's hereditary optic neuropathy. J Neurol Neurosurg Psychiatry 2001;70(4):444–449. [PubMed: 11254765]
14. Inglese M, Ghezzi A, Bianchi S, et al. Irreversible disability and tissue loss in multiple sclerosis: a conventional and magnetization transfer magnetic resonance imaging study of the optic nerves. Arch Neurol 2002;59(2):250–255. [PubMed: 11843696]
15. Hickman SJ, Toosy AT, Jones SJ, et al. Serial magnetization transfer imaging in acute optic neuritis. Brain 2004;127(Pt 3):692–700. [PubMed: 14736754]
16. Moore GR, Leung E, MacKay AL, et al. A pathology-MRI study of the short-T2 component in formalin-fixed multiple sclerosis brain. Neurology 2000;55(10):1506–1510. [PubMed: 11094105]

17. Laule C, Vavasour IM, Madler B, et al. MR evidence of long T2 water in pathological white matter. J Magn Reson Imaging 2007;26(4):1117–1121. [PubMed: 17896375]
18. Laule C, Leung E, Lis DK, et al. Myelin water imaging in multiple sclerosis: quantitative correlations with histopathology. Mult Scler 2006;12(6):747–753. [PubMed: 17263002]
19. Laule C, Vavasour IM, Moore GR, et al. Water content and myelin water fraction in multiple sclerosis. A T2 relaxation study. J Neurol 2004;251(3):284–293. [PubMed: 15015007]
20. Ou, X.; Sun, SW.; Gochberg, DK.; Song, SK. QMT is Specifically Sensitive to Myelin and Not Axonal Injury in Optic Nerve from Mice Undergoing Transient Retinal Ischemia. Berlin, Germany: 2007. p. 2377
21. Ou, X.; Sun, SW.; Liang, HF.; Gochberg, DK.; Song, SK. QMT Estimated Pool Size Ratio and DTI Derived Radial Diffusivity Reflect the Integrity of Myelin Sheath in Mice. Berlin, Germany: 2007. p. 317
22. Smith, SA.; van Zijl, PCM.; Raymond, GV.; Moser, HW.; Stanisz, GJ. Quantitative MT (qMT) Characteristics of the Human Spinal Cord In Vivo. Berlin, Germany: 2007. p. 2332
23. Le Bihan D, Mangin JF, Poupon C, et al. Diffusion tensor imaging: concepts and applications. J Magn Reson Imaging 2001;13(4):534–546. [PubMed: 11276097]
24. Huppi PS, Dubois J. Diffusion tensor imaging of brain development. Semin Fetal Neonatal Med 2006;11(6):489–497. [PubMed: 16962837]
25. Mori S, Zhang J. Principles of diffusion tensor imaging and its applications to basic neuroscience research. Neuron 2006;51(5):527–539. [PubMed: 16950152]
26. Song SK, Sun SW, Ju WK, Lin SJ, Cross AH, Neufeld AH. Diffusion tensor imaging detects and differentiates axon and myelin degeneration in mouse optic nerve after retinal ischemia. Neuroimage 2003;20(3):1714–1722. [PubMed: 14642481]
27. Song SK, Sun SW, Ramsbottom MJ, Chang C, Russell J, Cross AH. Dysmyelination revealed through MRI as increased radial (but unchanged axial) diffusion of water. Neuroimage 2002;17(3):1429–1436. [PubMed: 12414282]
28. Song SK, Yoshino J, Le TQ, et al. Demyelination increases radial diffusivity in corpus callosum of mouse brain. Neuroimage 2005;26(1):132–140. [PubMed: 15862213]
29. Sun SW, Liang HF, Trinkaus K, Cross AH, Armstrong RC, Song SK. Noninvasive detection of cuprizone induced axonal damage and demyelination in the mouse corpus callosum. Magn Reson Med 2006;55(2):302–308. [PubMed: 16408263]
30. Kim JH, Budde MD, Liang HF, et al. Detecting axon damage in spinal cord from a mouse model of multiple sclerosis. Neurobiol Dis 2006;21(3):626–632. [PubMed: 16298135]
31. Le Bihan D, Breton E, Lallemand D, Grenier P, Cabanis E, Laval-Jeantet M. MR imaging of intravoxel incoherent motions: application to diffusion and perfusion in neurologic disorders. Radiology 1986;161(2):401–407. [PubMed: 3763909]
32. Basser PJ, Pierpaoli C. Microstructural and physiological features of tissues elucidated by quantitative-diffusion-tensor MRI. J Magn Reson B 1996;111(3):209–219. [PubMed: 8661285]
33. Kingsley PB. Introduction to diffusion tensor imaging mathematics: Part II. Anisotropy, diffusion-weighting factors, and gradient encoding schemes. Concepts in Magnetic Resonance 2006;28A(2): 123–154.
34. Kanaan RA, Kim JS, Kaufmann WE, Pearlson GD, Barker GJ, McGuire PK. Diffusion tensor imaging in schizophrenia. Biol Psychiatry 2005;58(12):921–929. [PubMed: 16043134]
35. Mukherjee P. Diffusion tensor imaging and fiber tractography in acute stroke. Neuroimaging Clin N Am 2005;15(3):655–665. [PubMed: 16360595]xii
36. Ge Y, Law M, Grossman RI. Applications of diffusion tensor MR imaging in multiple sclerosis. Ann N Y Acad Sci 2005;1064:202–219. [PubMed: 16394158]
37. Wang S, Melhem ER. Amyotrophic lateral sclerosis and primary lateral sclerosis: The role of diffusion tensor imaging and other advanced MR-based techniques as objective upper motor neuron markers. Ann N Y Acad Sci 2005;1064:61–77. [PubMed: 16394148]
38. Lee SK, Kim DI, Kim J, et al. Diffusion-tensor MR imaging and fiber tractography: a new method of describing aberrant fiber connections in developmental CNS anomalies. Radiographics 2005;25 (1):53–65. [PubMed: 15653586]discussion 66-58

39. Field AS, Alexander AL. Diffusion tensor imaging in cerebral tumor diagnosis and therapy. Top Magn Reson Imaging 2004;15(5):315–324. [PubMed: 15627005]
40. Neil J, Miller J, Mukherjee P, Huppi PS. Diffusion tensor imaging of normal and injured developing human brain - a technical review. NMR Biomed 2002;15(78):543–552. [PubMed: 12489100]
41. Kubicki M, Westin CF, Maier SE, et al. Diffusion tensor imaging and its application to neuropsychiatric disorders. Harv Rev Psychiatry 2002;10(6):324–336. [PubMed: 12485979]
42. Kim JH, Loy DN, Liang HF, Trinkaus K, Schmidt RE, Song SK. Noninvasive diffusion tensor imaging of evolving white matter pathology in a mouse model of acute spinal cord injury. Magn Reson Med 2007;58(2):253–260. [PubMed: 17654597]
43. Sun SW, Liang HF, Schmidt RE, Cross AH, Song SK. Selective vulnerability of cerebral white matter in a murine model of multiple sclerosis detected using diffusion tensor imaging. Neurobiol Dis 2007;28(1):30–38. [PubMed: 17683944]
44. Helenius J, Soinne L, Salonen O, Kaste M, Tatlisumak T. Leukoaraiosis, ischemic stroke, and normal white matter on diffusion-weighted MRI. Stroke 2002;33(1):45–50. [PubMed: 11779887]
45. Sotak CH. The role of diffusion tensor imaging in the evaluation of ischemic brain injury - a review. NMR Biomed 2002;15(78):561–569. [PubMed: 12489102]
46. Stejskal EO, Tanner JE. Spin diffusion measurements: spin echoes in the presence of a time-dependent field gradient. J Chem Phys 1965;42:288–292.
47. Sun SW, Liang HF, Le TQ, Armstrong RC, Cross AH, Song SK. Differential sensitivity of in vivo and ex vivo diffusion tensor imaging to evolving optic nerve injury in mice with retinal ischemia. Neuroimage 2006;32(3):1195–1204. [PubMed: 16797189]
48. Sun S-W, Liang H-F, Cross AH, Song S-K. Evolving Wallerian degeneration after transient retinal ischemia in mice characterized by diffusion tensor imaging. Neuroimage. 2007In Press
49. Thelwall PE, Shepherd TM, Stanisz GJ, Blackband SJ. Effects of temperature and aldehyde fixation on tissue water diffusion properties, studied in an erythrocyte ghost tissue model. Magn Reson Med 2006;56(2):282–289. [PubMed: 16841346]
50. Sun SW, Neil JJ, Song SK. Relative indices of water diffusion anisotropy are equivalent in live and formalin-fixed mouse brains. Magn Reson Med 2003;50(4):743–748. [PubMed: 14523960]
51. Gupta RK, Saksena S, Hasan KM, et al. Focal Wallerian degeneration of the corpus callosum in large middle cerebral artery stroke: serial diffusion tensor imaging. J Magn Reson Imaging 2006;24(3): 549–555. [PubMed: 16888796]
52. Khong PL, Zhou LJ, Ooi GC, Chung BH, Cheung RT, Wong VC. The evaluation of Wallerian degeneration in chronic paediatric middle cerebral artery infarction using diffusion tensor MR imaging. Cerebrovasc Dis 2004;18(3):240–247. [PubMed: 15273442]
53. Thomalla G, Glauche V, Koch MA, Beaulieu C, Weiller C, Rother J. Diffusion tensor imaging detects early Wallerian degeneration of the pyramidal tract after ischemic stroke. Neuroimage 2004;22(4): 1767–1774. [PubMed: 15275932]
54. Thomalla G, Glauche V, Weiller C, Rother J. Time course of wallerian degeneration after ischaemic stroke revealed by diffusion tensor imaging. J Neurol Neurosurg Psychiatry 2005;76(2):266–268. [PubMed: 15654048]
55. Sun SW, Liang HF, Cross AH, Song SK. Evolving Wallerian degeneration after transient retinal ischemia in mice characterized by diffusion tensor imaging. Neuroimage 2008;40(1):1–10. [PubMed: 18187343]
56. Steinman L, Zamvil SS. How to successfully apply animal studies in experimental allergic encephalomyelitis to research on multiple sclerosis. Ann Neurol 2006;60(1):12–21. [PubMed: 16802293]
57. Lassmann H. Chronic relapsing experimental allergic encephalomyelitis: its value as an experimental model for multiple sclerosis. J Neurol 1983;229(4):207–220. [PubMed: 6192222]
58. Zamvil SS, Mitchell DJ, Moore AC, Kitamura K, Steinman L, Rothbard JB. T-cell epitope of the autoantigen myelin basic protein that induces encephalomyelitis. Nature 1986;324(6094):258–260. [PubMed: 2431317]
59. Tuohy VK, Lu Z, Sobel RA, Laursen RA, Lees MB. Identification of an encephalitogenic determinant of myelin proteolipid protein for SJL mice. J Immunol 1989;142(5):1523–1527. [PubMed: 2465343]

60. Greer JM, Kuchroo VK, Sobel RA, Lees MB. Identification and characterization of a second encephalitogenic determinant of myelin proteolipid protein (residues 178-191) for SJL mice. J Immunol 1992;149(3):783–788. [PubMed: 1378866]
61. Lyons JA, Ramsbottom MJ, Cross AH. Critical role of antigen-specific antibody in experimental autoimmune encephalomyelitis induced by recombinant myelin oligodendrocyte glycoprotein. Eur J Immunol 2002;32(7):1905–1913. [PubMed: 12115610]
62. Shindler KS, Guan Y, Ventura E, Bennett J, Rostami A. Retinal ganglion cell loss induced by acute optic neuritis in a relapsing model of multiple sclerosis. Mult Scler 2006;12(5):526–532. [PubMed: 17086896]
63. Bettelli E, Baeten D, Jager A, Sobel RA, Kuchroo VK. Myelin oligodendrocyte glycoprotein-specific T and B cells cooperate to induce a Devic-like disease in mice. J Clin Invest 2006;116(9):2393–2402. [PubMed: 16955141]
64. Wu Q, Butzkueven H, Gresle M, et al. MR diffusion changes correlate with ultra-structurally defined axonal degeneration in murine optic nerve. Neuroimage 2007;37(4):1138–1147. [PubMed: 17689104]
65. Barker GJ. Diffusion-weighted imaging of the spinal cord and optic nerve. J Neurol Sci 2001;186 (Suppl 1):S45–49. [PubMed: 11334989]
66. Kallenbach K, Frederiksen J. Optical coherence tomography in optic neuritis and multiple sclerosis: a review. Eur J Neurol 2007;14(8):841–849. [PubMed: 17662003]
67. Trick GL. Beyond visual acuity: new and complementary tests of visual function. Neurol Clin 2003;21 (2):363–386. [PubMed: 12916484]
68. Kupersmith MJ. Visual evoked potential: enhancing its utility. Semin Neurol 1986;6(2):217–230. [PubMed: 3332426]
69. Sokol S. Visually evoked potentials: theory, techniques and clinical applications. Surv Ophthalmol 1976;21(1):18–44. [PubMed: 785653]
70. Iwasawa T, Matoba H, Ogi A, et al. Diffusion-weighted imaging of the human optic nerve: a new approach to evaluate optic neuritis in multiple sclerosis. Magn Reson Med 1997;38(3):484–491. [PubMed: 9339450]
71. Chabert S, Molko N, Cointepas Y, Le Roux P, Le Bihan D. Diffusion tensor imaging of the human optic nerve using a non-CPMG fast spin echo sequence. J Magn Reson Imaging 2005;22(2):307–310. [PubMed: 16028249]
72. Freeman, AJ.; Ballinger, R.; Werner, M.; Guy, J. Diffusion weighted EPI of the human optic nerve at 3T. Sydney, Australia: 1998. p. 1265
73. Kumar, A.; Ven-Der-Kouwe, AJ.; Sorensen, AG.; Caruso, P. DTI of The Optic Nerve. Seattle, Washington, USA: 2006. p. 2715
74. Xu, J.; Snyder, AZ.; Foster, G.; Naismith, RT.; Cross, AH.; Song, SK. Optic Nerve Injury Increases Water Diffusivity. Seattle, Washington, USA: 2006. p. 3418
75. Wheeler-Kingshott CA, Parker GJ, Symms MR, et al. ADC mapping of the human optic nerve: increased resolution, coverage, and reliability with CSF-suppressed ZOOM-EPI. Magn Reson Med 2002;47(1):24–31. [PubMed: 11754439]
76. Hickman SJ, Wheeler-Kingshott CA, Jones SJ, et al. Optic nerve diffusion measurement from diffusion-weighted imaging in optic neuritis. AJNR Am J Neuroradiol 2005;26(4):951–956. [PubMed: 15814951]
77. Trip SA, Wheeler-Kingshott C, Jones SJ, et al. Optic nerve diffusion tensor imaging in optic neuritis. Neuroimage 2006;30(2):498–505. [PubMed: 16242968]
78. Wheeler-Kingshott CA, Trip SA, Symms MR, Parker GJ, Barker GJ, Miller DH. In vivo diffusion tensor imaging of the human optic nerve: pilot study in normal controls. Magn Reson Med 2006;56 (2):446–451. [PubMed: 16791864]
79. Xu, J.; Naismith, RT.; Trinkaus, KM.; Cross, AH.; Song, SK. Towards Accurate In Vivo Diffusion Measurement in Human Optic Nerve. Berlin, Germany: 2007. p. 11
80. Feinberg DA, Hoenninger JC, Crooks LE, Kaufman L, Watts JC, Arakawa M. Inner volume MR imaging: technical concepts and their application. Radiology 1985;156(3):743–747. [PubMed: 4023236]

81. Weaver JB, Harris RD, Spiegel PK. Limited field of view spin echo MR imaging. Magn Reson Imaging 1991;9(3):389–394. [PubMed: 1881258]
82. Jeong EK, Kim SE, Guo J, Kholmovski EG, Parker DL. High-resolution DTI with 2D interleaved multislice reduced FOV single-shot diffusion-weighted EPI (2D ss-rFOV-DWEPI). Magn Reson Med 2005;54(6):1575–1579. [PubMed: 16254946]
83. Reese TG, Heid O, Weisskoff RM, Wedeen VJ. Reduction of eddy-current-induced distortion in diffusion MRI using a twice-refocused spin echo. Magn Reson Med 2003;49(1):177–182. [PubMed: 12509835]
84. Dowell, NG.; Miller, DH.; Jenkins, T.; Wheeler-Kingshott, C. Contiguous-Slice Diffusion Tensor Imaging of the Optic Nerve with CSF Suppressed IR CO-ZOOM. Berlin, Germany: 2007. p. 10
85. Jeong EK, Kim SE, Kholmovski EG, Parker DL. High-resolution DTI of a localized volume using 3D single-shot diffusion-weighted STimulated echo-planar imaging (3D ss-DWSTEPI). Magn Reson Med 2006;56(6):1173–1181. [PubMed: 17089367]
86. Finsterbusch J, Frahm J. Diffusion tensor mapping of the human brain using single-shot line scan imaging. J Magn Reson Imaging 2000;12(3):388–394. [PubMed: 10992305]
87. Gudbjartsson H, Maier SE, Mulkern RV, Morocz IA, Patz S, Jolesz FA. Line scan diffusion imaging. Magn Reson Med 1996;36(4):509–519. [PubMed: 8892201]
88. Vinogradov E, Degenhardt A, Smith D, et al. High-resolution anatomic, diffusion tensor, and magnetization transfer magnetic resonance imaging of the optic chiasm at 3T. J Magn Reson Imaging 2005;22(2):302–306. [PubMed: 16028247]
89. Xu, J.; Song, SK. Diffusion Measurement of Human Optic Nerve Using Fat Suppressed Diffusion Turbo FLASH Sequence. Seattle, Washington, USA: 2006. p. 453
90. Koch MA, Glauche V, Finsterbusch J, et al. Distortion-free diffusion tensor imaging of cranial nerves and of inferior temporal and orbitofrontal white matter. Neuroimage 2002;17(1):497–506. [PubMed: 12482102]
91. Nolte UG, Finsterbusch J, Frahm J. Rapid isotropic diffusion mapping without susceptibility artifacts: whole brain studies using diffusion-weighted single-shot STEAM MR imaging. Magn Reson Med 2000;44(5):731–736. [PubMed: 11064408]
92. Rieseberg S, Merboldt KD, Kuntzel M, Frahm J. Diffusion tensor imaging using partial Fourier STEAM MRI with projection onto convex subsets reconstruction. Magn Reson Med 2005;54(2): 486–490. [PubMed: 16032668]
93. Chamberlain R, Park JY, Corum C, et al. RASER: a new ultrafast magnetic resonance imaging method. Magn Reson Med 2007;58(4):794–799. [PubMed: 17899612]
94. Breslau J, Dalley RW, Tsuruda JS, Hayes CE, Maravilla KR. Phased-array surface coil MR of the orbits and optic nerves. AJNR Am J Neuroradiol 1995;16(6):1247–1251. [PubMed: 7677017]
95. Gomori JM, Holland GA, Grossman RI, Gefter WB, Lenkinski RE. Fat suppression by section-select gradient reversal on spin-echo MR imaging. Work in progress. Radiology 1988;168(2):493–495. [PubMed: 3393670]
96. Volk A, Tiffon B, Mispelter J, Lhoste JM. Chemical shift-specific slice selectionn-a new method for chemical-shift imaging at high magnetic-field. J Magn Reson 1987;71:168–174.
97. Le Roux P. Non-CPMG Fast Spin Echo with full signal. J Magn Reson 2002;155(2):278–292. [PubMed: 12036339]
98. Wheeler-Kingshott, CAM.; Symms, MR.; Parker, GJM.; Hickman, SJ.; Miller, DH.; Barker, GJ. High-resolution CSF-suppressed diffusion measurement in the optic nerve in vivo. Denver, Colorado, USA: 2000. p. 548
99. Naismith, RT.; Xu, J.; Snyder, AZ., et al. Axial Diffusivity in Acute and Isolated Optic Neuritis. Toronto, Canada: 2008. p. 3392
100. Hasan KM, Narayana PA. Retrospective measurement of the diffusion tensor eigenvalues from diffusion anisotropy and mean diffusivity in DTI. Magn Reson Med 2006;56(1):130–137. [PubMed: 16755537]

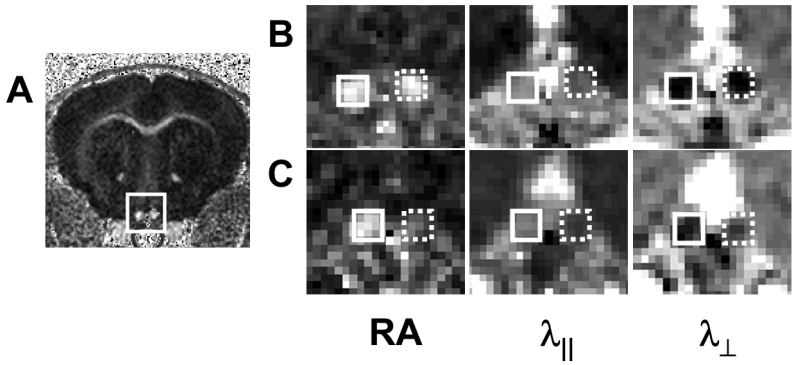

Figure 1.
Mouse optic nerves after one-hour transient retinal ischemia in right eye (reproduced from Sun *et al.*[47] Figure 1 with modification). Optic nerves (rectangle, A) appear hyperintense in a representative diffusion anisotropy, RA, map of a control mouse. Diffusion parameters maps of both control (solid rectangle) and injured (dashed rectangle) optic nerves on 3 (B) and 14 (C) days after retinal ischemia from a representative mouse demonstrating RA, $\lambda_{\parallel}$, and $\lambda_{\perp}$ changes after injury. Decreased $\lambda_{\parallel}$ was seen in the injured optic nerve at 3 and 14 days after retinal ischemia, while increased $\lambda_{\perp}$ was seen only at 14 days after retinal ischemia.

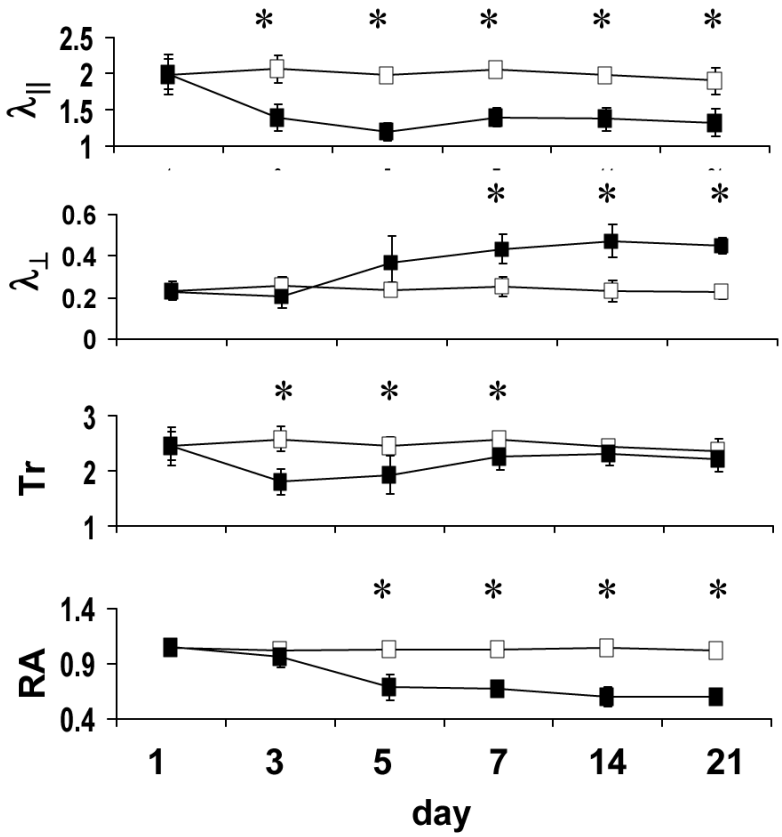

Figure 2.

Time course of DTI indices in the optic nerve obtained from mice after transient retinal ischemia (reproduced from Sun *et al.* [47] Figure 2 with modification). The filled and open squares are measurements obtained from the injured and control optic nerves, respectively. The $\lambda_{\parallel}$ of injured optic nerve decreased significantly at 3 days after reperfusion, remaining at this reduced value throughout the 21-day time course. The $\lambda_{\perp}$ of injured optic nerve increased and reached a plateau at 7 days. Decreased Tr was observed at 3 – 7 days as a consequence of reduced $\lambda_{\parallel}$. At 7 – 21 days, decreased $\lambda_{\parallel}$ and increased $\lambda_{\perp}$ resulted in the pseudo-normalized Tr. Relative anisotropy decreased at 5 days and remained at the level at 5 – 21 days. Tr, $\lambda_{\parallel}$, and $\lambda_{\perp}$ are in units of $\mu m^2/ms$. RA has no unit. "*" indicates statistically significant difference ($p < 0.05$) between the control and injured optic nerve.

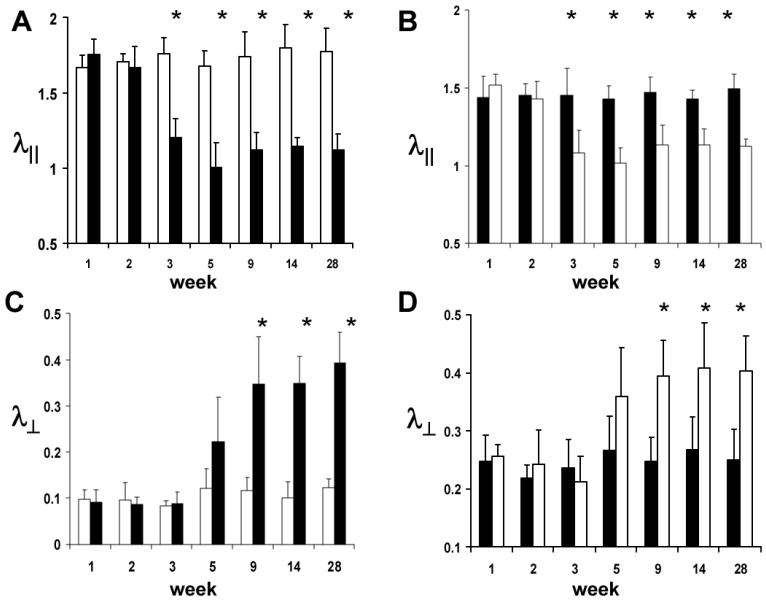

Figure 3.

Time courses of $\lambda_{\parallel}$ (A and B) and $\lambda_{\perp}$ (C and D) of the ipsilateral (filled bars) and contralateral (opened bars) optic nerve (A and C) and tract (B and D) after transient retinal ischemia obtain from a group of mice (N = 6). (Reproduced from Sun *et al.* [55]Figure 4 with modification.) Bars are mean ± standard deviation. Decreased $\lambda_{\parallel}$ was observed at 3 – 28 days from both ipsilateral optic nerve and contralateral optic tract, suggestive of the axonal damage. Increased $\lambda_{\perp}$ was also observed at 9 – 28 days from both ipsilateral optic nerve and contralateral optic tract, suggestive of myelin damage. The horizontal axis represents days after retinal ischemia. The units for $\lambda_{\parallel}$ and $\lambda_{\perp}$ are $\mu m^2/ms$. "*"indicates a statistically significant difference ($p < 0.05$) between the ipsilateral and contralateral optic nerve. The relative extent of changes in optic nerves is more profound than those in optic tracts, suggesting the more severe injury in the tract proximal to the source of insult than in the tract distant to it.

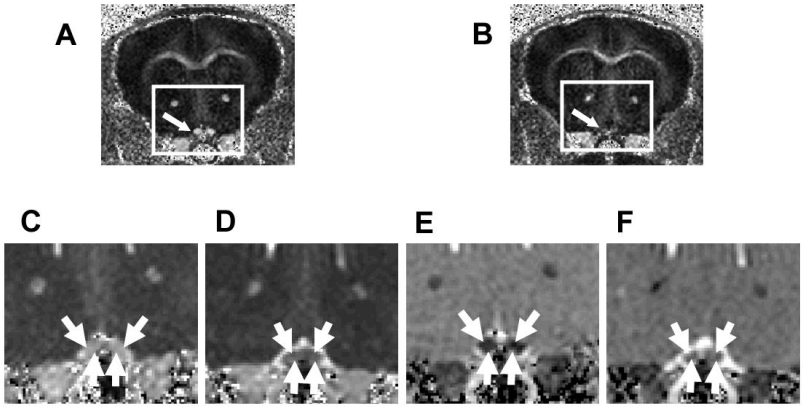

Figure 4.

Optic nerves (indicated by arrows) from the EAE-affected mouse appears hypointense (B) in RA maps, comparing to the control (A). Decreased $\lambda_{\parallel}$ (D) and increased $\lambda_{\perp}$ (F) in optic nerves from EAE-affected mice were observed in the expanded views of $\lambda_{\parallel}$ (C and D) and $\lambda_{\perp}$ (E and F) corresponding to the rectangles in (A) and (B). (Reproduced from Sun *et al.* [55] Figures 2 and 3 with modification.)

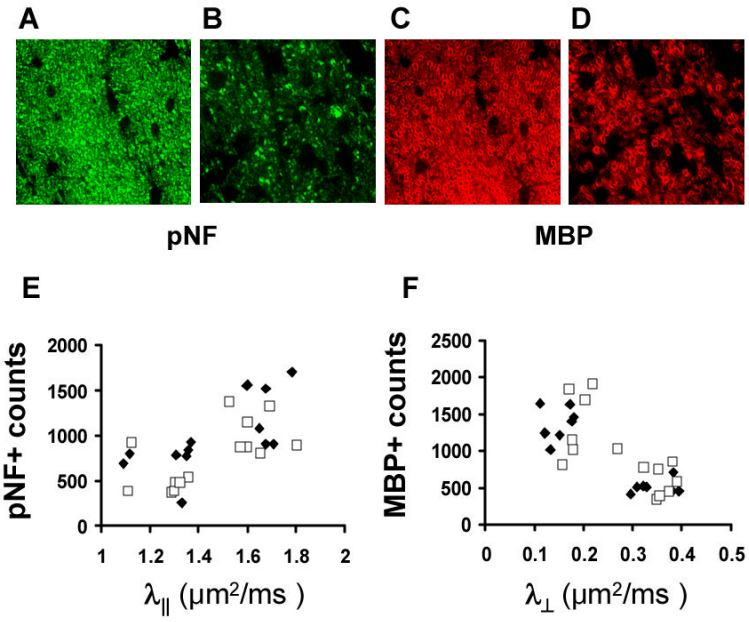

Figure 5.

Immunohistochemistry of pNF (A and B) and MBP (C and D) of optic nerves from control (A and C) and EAE-affected (B and D) mice (reproduced from Sun *et al.* [43] Figures 6 and 7 with modification). Axonal and myelin injury is seen as reduced pNF and MBP staining, as well as the significant change in axonal morphology in the optic nerve from the EAE-affected mice. The $\lambda_{\parallel}$ correlates with pNF positive axonal counts (E). Similarly, the $\lambda_{\perp}$ inversely correlates with MBP positive axonal counts (F).

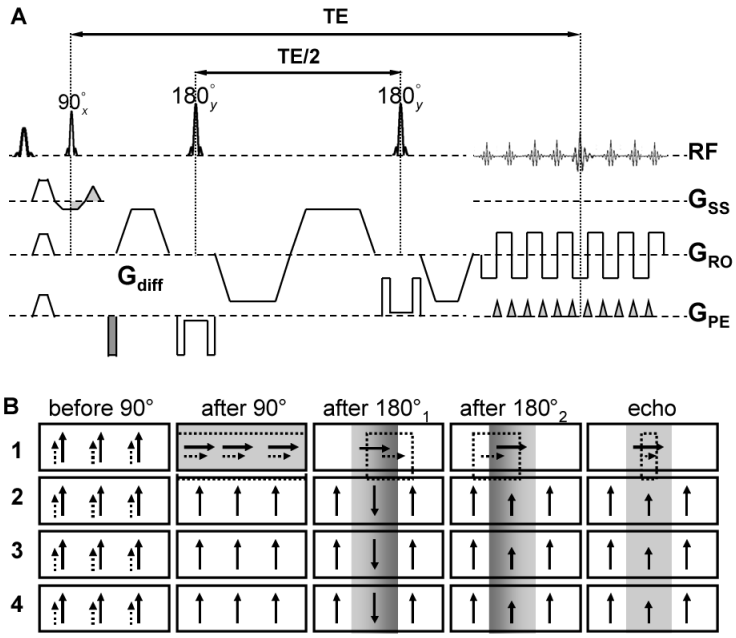

Figure 6.

The top panel (A) shows a single shot SE-EPI sequence implemented with inner volume imaging (IVI) and twice refocused spin echo (TRSE) diffusion weighting. Note the 180° pulses are selective in the phase encoding (G_{pe}) direction. The direction of the diffusion sensitive gradients (G_{diff}) is arbitrary. The bottom panel (B) illustrates the magnetization evolution (adapted from Figure 1b in Jeong *et al.* [82]) with gradient reversal technique. The shaded boxes represent the excited/refocused water slice/slab while the dashed boxes represent shifted fat slice/slab. The solid arrows and dashed arrows represent water and residual fat magnetization due to imperfect fat saturation, respectively. The fat signal (only the slice of interest is shown after the 90° excitation pulse) is greatly decreased at the time of echo formation. The effectiveness of the gradient reversal technique increases with the ratio of fat-water frequency difference to the bandwidth of the slab selective 180° refocusing/inversion pulses.

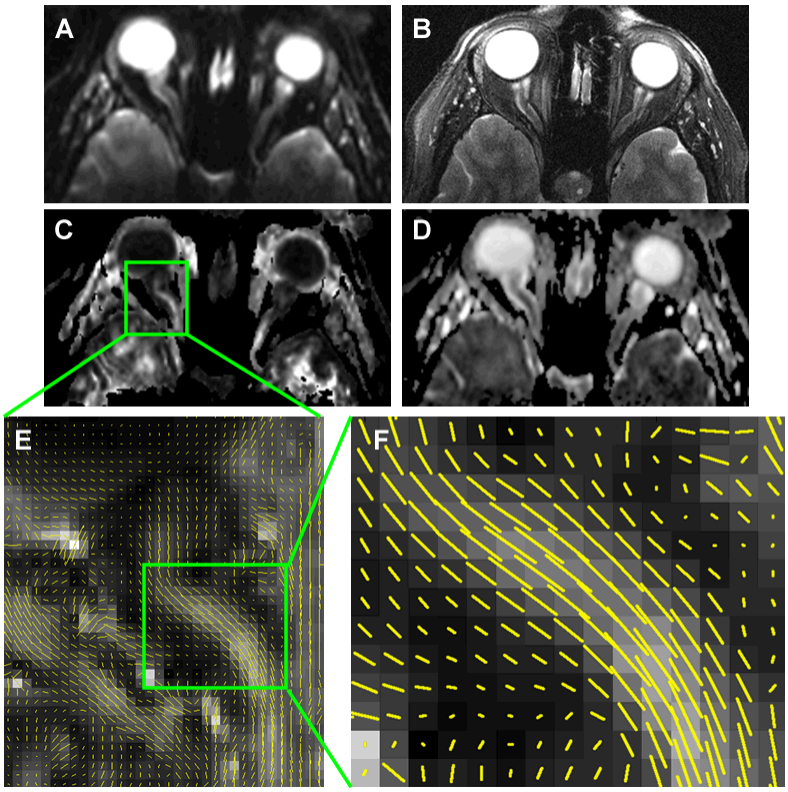

Figure 7.
Human optic nerve images from a normal subject with substantial nerve curvature illustrating high quality diffusion images achieved with the IVI diffusion sequence/protocol. A) b_0, B) T_2W, C) FA, D) MD, E) whisker plot, and F) magnified whisker plot. Little susceptibility artifacts and blurring were observed in b_0 image and DTI index maps comparing to the T_2W image. Clear delineation can be seen between the nerve and the surrounding CSF. Whisker plots, showing the projection of the principal eigenvector in each voxel overlaying the FA map, demonstrate the fiber coherence despite the curvature of the subject's optic nerve.

Table 1

Summary of normal human optic nerve DTI indices in literatures from three different groups.

	$\lambda_{\parallel}$ ($\mu m^2/ms$)	$\lambda_{\perp}$ ($\mu m^2/ms$)	MD ($\mu m^2/ms$)	FA	Resolution (mm^3)	Fat Suppr	CSF Suppr	Diffusion Sequence
Trip et al [77] (n=15)	2.09±0.31	0.63±0.20	1.08±0.17	0.67±0.09	1.25×1.25×4=6.25	Y	Y	ZOOM-EPI
Wheeler-Kingshot et al [78] (n=10)	2.10±0.21	0.86±0.25	1.22±0.20	0.61±0.10	1.25×1.25×4=6.25	Y	Y	ZOOM-EPI
Chatbert et al [71] (n=7)	1.78±0.21†	0.76±0.19†	1.10±0.20	0.49±0.06	0.94×0.94×3=2.65	N	N	non-CPMG FSE
Naismith, Xu et al [79] (n=12)	1.66±0.18	0.81±0.26	1.09±0.21	0.46±0.15	1.3×1.3×1.3=2.20	Y	N	IVI-EPI

† indicates directional diffusivities derived from MD and FA retrospectively [100].